Vibrationally Induced Interconversion of H-Bonded $NO_2^-\cdot H_2O$ Isomers within $NO_2^-\cdot H_2O\cdot Ar_m$ Clusters Using IR−IR Pump−Probe through the OH and NO Stretching Vibrations

Rachael A. Relph, Ben M. Elliott, Gary H. Weddle,† and Mark A. Johnson*

Sterling Chemistry Laboratory, Yale University, P.O. Box 208107, New Haven, Connecticut 06520

Jing Ding and Kenneth D. Jordan*

Department of Chemistry, University of Pittsburgh, Pittsburgh, Pennsylvania 15260

Received: September 17, 2008; Revised Manuscript Received: December 1, 2008

We introduce a method based on sequential application of vibrational predissociation spectroscopy to explore the high-amplitude rearrangements available in a small H-bonded complex that is vibrationally excited within a larger Ar cluster. The weakly bound Ar atoms play the role of a solvent in mediating the energy content of the embedded system, ultimately quenching it into local minima through evaporation. We demonstrate the approach on the $NO_2^-\cdot H_2O$ binary hydrate, which is known to occur in two nearly isoenergetic isomeric forms. The scheme involves three stages of mass separation to select a particular $NO_2^-\cdot H_2O\cdot Ar_m$ parent ion cluster prior to vibrational excitation and then isolate the $NO_2^-\cdot H_2O\cdot Ar$ fragment ions for interrogation using resonant vibrational predissociation with a second infrared laser. The initial vibrational excitation selectively energizes one of the isomers through one of its characteristic resonances while the predissociation spectrum of the $NO_2^-\cdot H_2O\cdot Ar$ fragment encodes the distribution of isomers present after Ar evaporation. Isomerization from the front- to backside form is found to occur upon excitation of the NO stretch near 1200 cm^{-1}; although the reverse reaction is not observed upon excitation of the NO stretch, it is observed upon excitation of the higher-energy OH stretching fundamental near 3000 cm^{-1}. We discuss these observations in the context of the calculated isomerization energetics, which focus on the minimum energy structures for the isomers as well as the transition states for their interconversion.

I. Introduction

Vibrational predissociation spectroscopy of mass-selected ion clusters is emerging as the method of choice for the structural characterization of ion−solvent complexes, where weakly bound messenger species such as Ar atoms are used to record absorption in an action mode via mass loss.[1] This has been particularly useful in elucidating the structures of the hydration shells around simple ions, with the halide ions representing a classic case in which all six of the fundamentals associated with $X^-\cdot H_2O$ have been observed experimentally.[2−7] In many cases, however, the strength and directionality of the H-bond leads to many isomeric structures in the ionic hydrates, $A^{-/+}\cdot(H_2O)_n$.[8−11] This circumstance has presented a complication in spectroscopic studies attempting to characterize minimum energy structures because one is routinely faced with sorting out extra bands that arise from anharmonic effects (Fermi resonances, combination bands, etc.) of a particular isomer from the heterogeneous contributions of distinct species. To address this complexity, we have recently developed a general method for obtaining isomer-specific spectra within the context of a mass-selective, predissociation-based variant of two-dimensional IR spectroscopy.[12] With the vibrational signatures of the various isomers in hand, we are now in an excellent position to exploit this knowledge to explore significant features on the extended potential energy landscape, such as barriers to isomer interconversion. In this context, the occurrence of the isomers becomes an advantage because they provide benchmarks that reveal the range of the excursions available from various starting points on the surface. We report here an extension of our IR-IR hole burning method[12] to monitor vibrationally induced isomerization within a size-selected Ar cluster. In essence, the attached Ar atoms play the role of solvent in that they mediate the energy content of a tightly bound core ion complex through intra- and intermolecular vibrational relaxation IVR and ultimately quench the clusters into local minima by evaporative cooling. This scheme can be viewed as an Ar-cluster variation on the collisionally mediated photoisomerization method developed for neutral complexes by Zwier and co-workers[13] over the past several years. The significant differences in its application to ionic clusters are that in the clusters, quenching occurs by Ar evaporation rather than through bimolecular collisions, and predissociation is used instead of resonant multiple photon ionization to carry out the spectroscopic characterization of the isomers present after excitation. We demonstrate the method on the $NO_2^-\cdot H_2O$ binary cluster, which occurs in two low-energy isomeric forms that were spectroscopically characterized in our earlier report.[12]

The strategy of our approach is illustrated schematically in Figure 1, which depicts the situation at play in $NO_2^-\cdot H_2O$. The two isomers have the calculated structures (B3LYP[14−17]/aug-cc-pVDZ[18,19]) indicated at the bottom of the figure. Isomer A is the "backside" form in which the water molecule docks primarily to one oxygen atom on NO_2^- in a single ionic H-bonding arrangement such that

* To whom correspondence should be addressed. E-mail: (M.A.J.) mark.johnson@yale.edu.; (K.D.J.) jordan@a.psc.edu.

† Current address: Department of Chemistry, Fairfield University, Fairfield, CT.

10.1021/jp808283r CCC: $40.75
Published on Web 01/16/2009

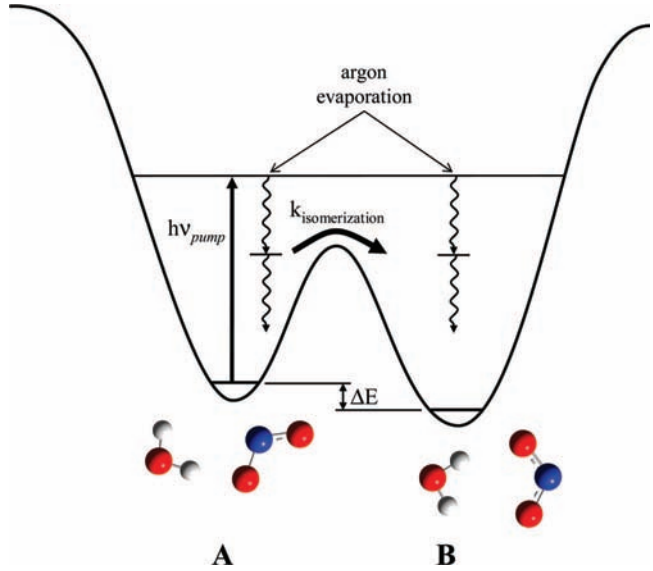

Figure 1. Schematic illustration of the Ar cluster-mediated approach to vibrationally induced intracluster photoisomerization. Isomer-selective vibrational excitation is carried out by a fixed frequency pump laser ($h\nu_{pump}$), which is sufficiently energetic to photoeject several Ar atoms. When the parent cluster is chosen such that at least one Ar atom remains on the daughter ions, the isomeric composition of these fragments can be established by obtaining their vibrational predissociation spectra (after mass selection) with a second infrared laser. Photoisomerization in this regime thus requires that the isomerization rate (k_{isom}) is sufficiently fast to compete with the evaporation rate of the weakly bound Ar atoms.

the "free" H atom is oriented toward the N atom. Isomer B is the so-called "frontside" form, in which the water molecule attaches each of its hydrogen atoms to the oxygen atoms on the NO_2^- ion in a double H-bonded configuration.

In this photoisomerization scheme, a particular isomer is selectively excited through one of its characteristic vibrational transitions within a mass-selected $NO_2^-\cdot H_2O\cdot Ar_m$ cluster. This energized cluster then undergoes IVR, ultimately leading to photoevaporation of one or more weakly bound Ar atoms ($n_{evap} \approx h\nu/\Delta H_{evap}$ (Ar)), which is the essential feature of the popular "tagging" approach for obtaining mass-selective vibrational spectra of ions.[1,20] Here we are interested in the case in which the vibrationally excited core ion can undergo isomerization before the energy is lost to evaporation, a process described by the following kinetic scheme:

$$^{I,II}[NO_2^-\cdot H_2O]\cdot Ar_m + h\nu^{I}_{pump} \rightarrow {}^{I}[NO_2^-\cdot H_2O]^{\dagger}\cdot Ar_m \xrightarrow{k_{evap}} {}^{I}[NO_2^-\cdot H_2O]\cdot Ar_{n(I)} + (m-n(I))Ar \quad (1a)$$

$$\xrightarrow{k_{isom}} {}^{II}[NO_2^-\cdot H_2O]^{\dagger}\cdot Ar_m \xrightarrow{k_{evap}} {}^{II}[NO_2^-\cdot H_2O]\cdot Ar_{n(II)} + (m-n(II))Ar \quad (1b)$$

where the superscripts I and II denote the two $NO_2^-\cdot H_2O$ isomeric cores, $h\nu^{I}_{pump}$ indicates that the pump laser is tuned to a resonance associated exclusively with isomer I, and $(m - n(I))$, $(m - n(II))$ denote the number of Ar atoms lost upon formation of the quenched isomers I and II, respectively. The initial $NO_2^-\cdot H_2O\cdot Ar_m$ cluster is chosen to contain a sufficiently large number (m) of attached Ar atoms such that at least one Ar atom remains attached after the photofragmentation induced by the pump laser. This is important because one can then monitor the predissociation spectra of the primary photofragments,

$$^{I,II}[NO_2^- \cdot H_2O]\cdot Ar_{n(I,II)} + h\nu_{probe} \rightarrow {}^{I,II}[NO_2^- \cdot H_2O] + n(I, II)Ar \quad (2)$$

as a means of establishing the isomer distribution present in the fragment ion ensemble. Although not illustrated above, it is clearly also possible that isomerization can occur during the course of Ar evaporation.

A key requirement of this approach is that k_{isom} is sufficiently fast to compete with evaporative energy loss, k_{evap}. Although one anticipates that IVR within a strongly H-bonded complex will be fast compared to the rate of Ar evaporation, these rates are not generally known in ion clusters.[21,22] As such, one of our primary goals in this study is to clarify whether isomerization can be observed in this intracluster regime. We will demonstrate that efficient interconversion does, indeed, occur between the $NO_2^-\cdot H_2O$ isomers; moreover, this transformation occurs in a fashion that depends strongly on the vibrational mode excited and, thus, the energy delivered to the cluster. This dependence is considered in the context of the calculated transition states for migration of the water molecule around the NO_2^- anion.

II. Experimental Details

Figure 2 outlines the protocol of the pump−probe approach. Two tunable infrared lasers intersect a pulsed ion beam at two of the three mass-selective, transient foci of the mass spectrometer, which are created using two pulsed fields and a reflectron. To implement this capability, the Yale double-focusing, tandem TOF photofragmentation spectrometer[23] was lengthened by about 1.5 m to accommodate a coaxial, pulsed acceleration region (located about 50 cm beyond the pump laser intersection at the first transient focus (F1)), followed by a second reflectron, R2. These features enable mass separation of the species created by the first laser at

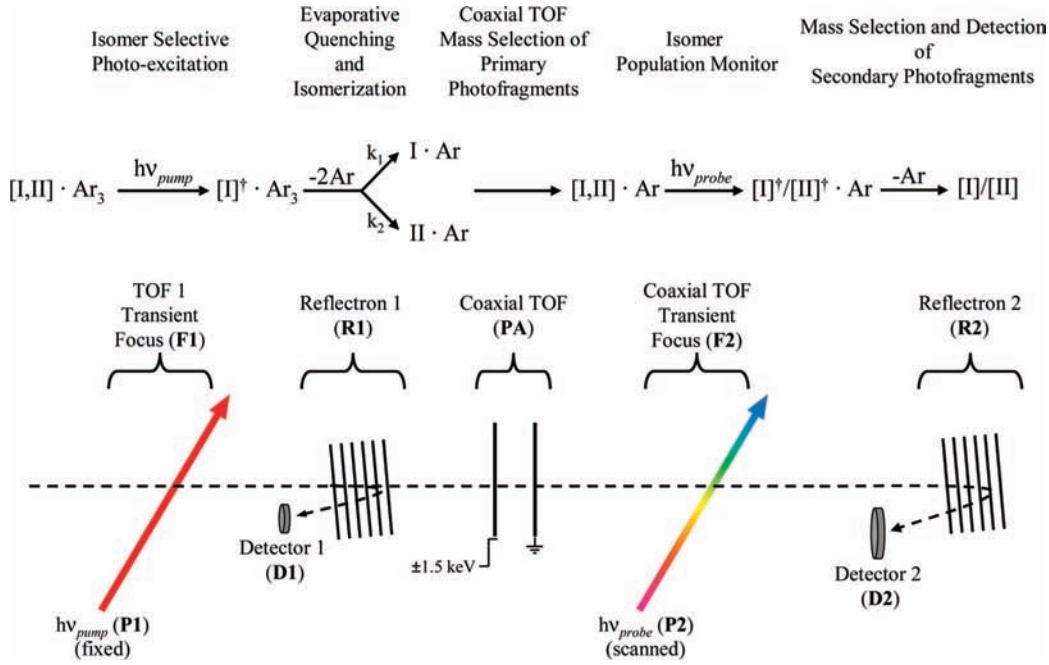

Figure 2. Outline of the experimental sequence of events used to carry out Ar-mediated, intracluster photoisomerization. An ion packet containing a mixed ensemble of isomers is mass-selected in the first stage of a time-of-flight (TOF) mass spectrometer, where a fixed frequency pump laser (P1) is tuned to a transition of one of the isomers and injects this species with vibrational energy, $h\nu_{pump}$. This interaction is optimized by monitoring the fragments on reflectron R1 with detector D1. After optimization, R1 is turned off, allowing the parent and daughter ion packets to pass without discrimination. If isomerization occurs, argon evaporation quenches the excited cluster into minima corresponding to the different isomeric forms. To characterize the isomer composition in the fragment ions, they are isolated from the parents remaining after pump excitation in a second (coaxial) TOF stage of mass selection using a pulsed acceleration (PA) region. A second tunable IR laser (the probe laser, P2) intersects the fragment ion packet at the transient focus of the second TOF stage. The predissociation spectrum arising from the scanned probe laser is recovered by detecting the resulting Ar loss detector D2 after a third stage of TOF mass selection using reflectron R2.

a second transient focus (F2), where a second tunable IR laser interrogates photofragments created by the pump laser. Fragments produced by the probe laser are then isolated using reflectron R2, which has an MCP ion detector (D2) located at the resulting third focal point. The overall assembly is equivalent to an MS^3 fragmentation experiment in the parlance of analytical mass spectrometry.

When carrying out the measurement, the pump laser is tuned to an isolated band assigned to one of the $NO_2^- \cdot H_2O$ isomers, and the efficiency of the excitation is maximized by monitoring the resulting photofragments on detector D1 with reflectron R1.

R1 is then switched off, sending the remaining parent and photofragment ions together down the drift tube. This mixed-mass ion packet is then separated by a pulsed, coaxial field, labeled PA in Figure 2, which is switched on just after the ion packet enters the region between the grids (7 cm separation). The grid closest to the ion source is typically pulsed from ground to −1.5 kV, with the remaining electrode held at ground. As such, the kinetic energies of all ions in the packet are increased by ∼1.5 keV. Parent and daughter ions from the pump laser are thus separated in this second TOF step, and the probe laser is timed to selectively intercept the daughter fragment created in the first predissociation event that retains one Ar atom (eq 2). Scanning the probe laser recovers the predissociation spectrum of these fragments, and the resulting bands reveal its isomeric composition.

The $NO_2^- \cdot H_2O \cdot Ar_m$ clusters were generated by entraining[24] NO_2 and H_2O on the low-pressure side of a pulsed supersonic expansion of Ar that was ionized with a 1 keV counter-propagating electron beam. The laser pulse energies used in this work were ∼10 mJ in the 2800−3800 cm^{-1} range, and 0.3−0.6 mJ in the 1000−2000 cm^{-1} range, where the latter region was obtained by secondary conversion in $AgGaSe_2$.[25,26] The reported spectra result from the accumulation of 10−30 scans.

III. Results and Discussion

We illustrate the method through its application to the $NO_2^- \cdot H_2O$ cluster ion, which is fortuitously prepared with comparable yields of the back- and frontside isomers (A and B in Figure 1, respectively) in the ionized free-jet cluster source.[12] The vibrational predissociation spectrum of the $NO_2^- \cdot H_2O \cdot Ar$ cluster, presented in Figure 3a, thus consists of two overlapping patterns. In discussing the assignments of the various bands, we make use of the results of reference 12 where ion-dip spectroscopy was used to separate the contributions of the two isomers. The contributions from each isomer are indicated in color, with blue representing the backside isomer and red indicating bands from the frontside isomer. The bands above 2500 cm^{-1} are derived from the OH stretching vibrations. The backside species contributes the strong ionic hydrogen-bonded (IHB) OH stretch (ν_{OH}^{IHB}(back)) at 2975 cm^{-1} along with a weaker nonbonded OH stretch (ν_{OH}^{free}(back)) near 3700 cm^{-1}. The backside isomer also contributes a broad feature near 3200 cm^{-1}, which may be a combination band involving the 2975 cm^{-1} fundamental and an ion−water molecule stretching vibration (calculated at the B3LYP/aug-cc-pVDZ level to occur at 242 cm^{-1}). The OH stretching pattern of the frontside species consists of a long progression of peaks evolving to higher energy relative to a band origin at 3250 cm^{-1}, with a characteristic spacing of about 90 cm^{-1}. We have previously discussed[8,27] the origin of this pattern in the context of combination band structure involving the OH stretching fundamentals with the rocking motion of the water molecule between the two oxygen atoms of NO_2^-. Qualitatively, the progression can be viewed in a

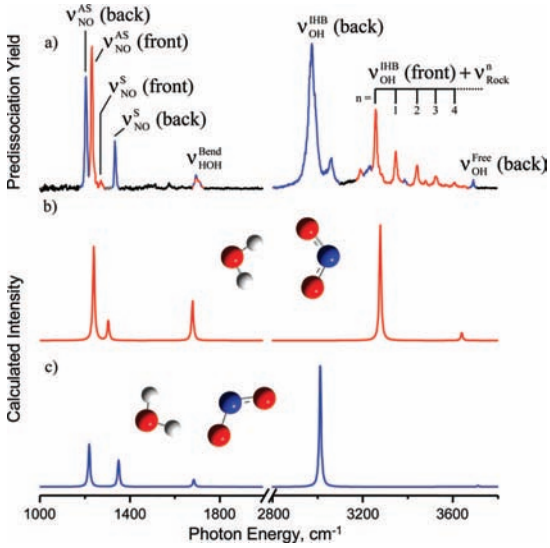

Figure 3. Vibrational predissociation and calculated (harmonic, B3LYP/aug-cc-pVDZ) spectra of $NO_2^-\cdot H_2O\cdot Ar$ in the NO stretching and OH stretching regions (from ref 12): (a) nonisomer selective predissociation spectrum with those peaks belonging to the frontside isomer in red and those for the backside isomer in blue, (b) calculated spectrum of the frontside isomer, and (c) calculated spectrum of the backside isomer. Structures indicate the calculated minimum energy geometries.

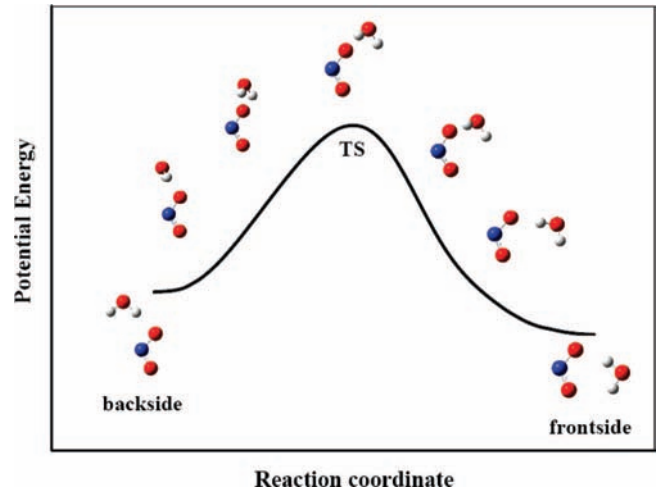

Figure 4. Reaction path for isomerization of $NO_2^-\cdot H_2O$. The TS was located using the QST3 method, as described in the text, and the reaction paths from the transition state to the two minima were established using the reaction path following method. The calculations are at the MP2/aug-cc-pVDZ level of theory.

Franck−Condon picture, where the shapes of the vibrationally adiabatic potentials for the rocking motion are strongly dependent on the number of quanta in the OH stretching vibration. This leads to displaced potentials for the rocking mode levels in going from $v_{OH} = 0$ to $v_{OH} = 1$ (in a local mode description), which in turn gives rise to overlap of the ground vibrational state with many v_{rock} levels upon excitation of the OH stretching fundamental.

The lower energy region of the predissociation spectrum is dominated by sharp bands arising from the NO stretches, where each isomer contributes two such bands. Most convenient for this study are the two very close bands near 1200 cm^{-1}, where the lower-energy 1203 cm^{-1} band is due to the backside isomer and the higher energy 1230 cm^{-1} band arises from the frontside isomer. This leads to a favorable situation in which one can manipulate the isomer populations by tuning the pump laser between these two closely spaced transitions.

IIIA. Theoretical Details and Expectations. To aid in the assignment of the spectra and in interpreting the isomerization dynamics, we have carried out an exhaustive search for stationary points on the $NO_2^-\cdot H_2O$ potential energy surface at the MP2[28]/aug-cc-pVDZ level of theory. The QST3 procedure[29] was employed to locate the transition state structures. For each stationary point identified, the vibrational frequencies were calculated in the harmonic approximation, again using the MP2/aug-cc-pVDZ method, to confirm the nature of the stationary points. The geometries of the minima were also optimized, and the harmonic vibrational frequencies were calculated at the B3LYP/aug-cc-pVDZ level of theory. Although the frequencies from the two sets of calculations are quite similar, the two theoretical methods give very different IR intensities, particularly for the NO stretch bands, with the results from the B3LYP calculations being in closer agreement with experiment. B3LYP calculations on the isolated NO_2^- ion reveal that the symmetric NO stretch lies higher in frequency than the asymmetric NO stretch, in agreement with experiment.[30] The opposite ordering of these two vibrations is found with the MP2 method, presumably due to the inadequacy of the Hartree−Fock reference configuration for describing the diradical character of NO_2^-. For this reason, the B3LYP results have been used in analyzing the spectra. Figures 3b and c report the calculated (B3LYP/aug-cc-pVDZ, scaled, harmonic) vibrational spectra for the frontside and backside isomers, respectively. Overall, the measured fundamentals are recovered quite well at the harmonic level for this method, with the most significant difference being the greater number of lines in the experimental spectra resulting from anharmonic couplings.

Both the B3LYP/aug-cc-pVDZ and MP2/aug-cc-pVDZ calculations predict the frontside isomer to be about 240 cm^{-1} more stable than the backside isomer after correction for vibrational zero-point energies. We also carried out single-point MP2/aug-cc-pVTZ, CCSD(T)[31−35]/aug-cc-pVDZ, and multireference MP2 (MRMP2)[36]/aug-cc-pVDZ calculations on the two low-energy minima, employing the MP2/aug-cc-pVDZ geometries. (The MRMP2 calculations employed the two references needed to account for the diradical nature of NO_2^-.) The B3LYP and MP2 calculations were carried out with the Gaussian 03 program,[37] and the CCSD(T) and MRMP2 calculations were carried out using MOLPRO.[38] The adoption of the more flexible basis set proves to have a negligible effect on the relative energies of the front and backside isomers. On the other hand, the CCSD(T) and CASMP2 calculations favor the frontside isomer by 417 cm^{-1}, as compared to by 240 cm^{-1} in the MP2 or B3LYP calculations. It is clear from these results that the frontside and backside isomers of $NO_2^-\cdot H_2O$ are close in energy.

If the energy ordering of the two isomers from the calculations described above is indeed correct, then the energy threshold for backside-to-frontside isomerization would be lower than that for the reverse reaction. It is therefore of interest that the experimental results presented below are consistent with a lower threshold for the frontside-to-backside process, raising the possibility that the observed rates reflect the detailed dynamics underlying the relative k_{isom} and k_{evap} rates.

The potential energy surface describing even a simple situation, such as the $NO_2^-\cdot H_2O$ interaction, is surprisingly complex, but the calculations suggest that the key reaction pathway is that shown in Figure 4. This path is essentially passage of the water molecule around one of the oxygen atoms in NO_2^- with concomitant rotation of one of the hydrogen atoms.

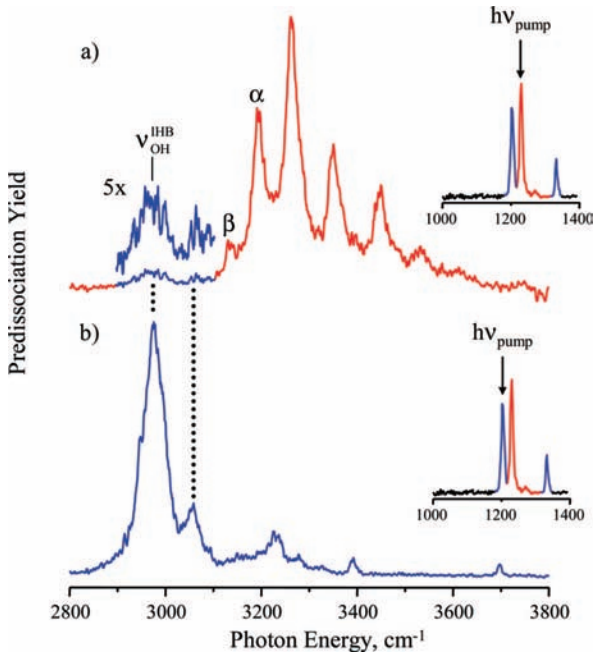

Figure 5. Argon predissociation spectra of the primary photofragment, $NO_2^-\cdot H_2O\cdot Ar$, produced from photoexcitation of $NO_2^-\cdot H_2O\cdot Ar_3$ with $h\nu_{pump}$ at (a) 1230 cm^{-1}, a frontside isomer transition, and (b) 1203 cm^{-1}, a backside isomer transition, as indicated in the insets. For the frontside isomer in part a, features assigned to hot bands are labeled α and β and represent transitions to $v'_{rock} = 0$ from excited v_{rock} levels in the OH ($v = 0$) level. See the vibrationally adiabatic potential discussion in the text. The presence of the backside ν_{OH}^{IHB} transition at 2975 cm^{-1} in part a indicates a small amount of conversion from frontside to backside, whereas the lack of any frontside features in part b indicates that excitation of the NO stretch does not induce conversion from the backside form to the frontside.

The transition state structure is calculated to lie 1163 and 919 cm^{-1} above the frontside and backside isomers, respectively. (These numbers are based on MP2 calculations.)

IIIB. Isomer Conversion through the NO Stretching Modes. We begin by investigating whether the isomers can undergo interconversion upon excitation of the ~1200 cm^{-1} NO stretching vibrations, which should provide internal energy just above the calculated barrier for the path in Figure 4. Previous studies have established that photofragmentation of Ar-tagged clusters at this energy is dominated by the loss of two Ar atoms.[24,39,40] We therefore focus on the $NO_2^-\cdot H_2O\cdot Ar_3$ parent ion, which should preferentially yield the $NO_2^-\cdot H_2O\cdot Ar$ fragment ion upon excitation of the NO stretching vibrations of either isomer in the absence of isomerization. Experimentally, we observe $NO_2^-\cdot H_2O\cdot Ar$ to be the dominant fragment upon excitation of either isomer. The presence of the Ar tag allows us to determine the isomeric composition of this photofragment by predissociation spectroscopy. To maximize the signal in the isomer analysis step, we probed the fragment ions in the OH stretching region where high laser power is available in the 3000−4000 cm^{-1} range.

Figure 5 presents the predissociation spectra of the $NO_2^-\cdot H_2O\cdot Ar$ fragment ions, where the top trace corresponds to excitation of the frontside isomer at 1230 cm^{-1} (indicated by the arrow in the Figure 5a inset), and the bottom trace results from excitation of the backside isomer through its 1203 cm^{-1} band (arrow in Figure 5b inset). The main qualitative message from this experiment is that the isomeric parentage is largely maintained upon excitation in this energy range. In fact, the lower trace, corresponding to selective excitation of the backside isomer, contains no bands attributable to contamination from the frontside isomer. The scan in Figure 5b is thus the most definitive spectrum of this species yet recorded, with all features previously assigned to the backside isomer using double resonance being present. Although photoisomerization starting from the backside species is not observed through the NO stretches, this observation illustrates a powerful (if unanticipated) use for the double resonance method as a means with which to isolate the linear action spectrum of a particular isomer. That is, once the fragment ion is created in a pure isomeric form with an Ar tag, its spectrum can be obtained using predissociation in a low laser power regime, as opposed to the saturated conditions that are intrinsic to the hole-burning approach.

We next turn to the photoexcited frontside isomer through its NO stretching transition at 1230 cm^{-1} (arrow in Figure 5a inset). This is a more interesting result than that obtained for the backside isomer in that, although the characteristic progression is evident as expected for the frontside pattern, there are two additional peaks toward the low-energy side, labeled α and β in Figure 5b, that were very weak (α) or absent (β) in the $NO_2^-\cdot H_2O\cdot Ar$ spectrum (top trace in Figure 3) when this ion was extracted as a parent directly from the ion source. In addition, there is a small feature at 2975 cm^{-1}, the location of the strong band associated with the backside isomer, suggesting that isomer interconversion can be induced in this direction.

Interestingly, the spacing between the enhanced peaks (α and β) as well as between α and OH stretching fundamental at 3250 cm^{-1} is about 65 cm^{-1}, which is even lower in energy than that (~90 cm^{-1}) displayed by the main progression associated with the rocking mode of the water molecule. Recall that the Franck−Condon mechanism for the ($0 \rightarrow v'_{rock}$) progression involves large displacements of the vibrationally adiabatic potentials describing the water-rocking motion upon OH-stretching excitation.[27] In this context, a natural explanation for the new bands is that they are due to ($v''_{rock} \rightarrow 0$) hot bands in this mode, which gain oscillator strength through the same Franck−Condon mechanism.[27] Activity in the ≈65 cm^{-1} quantum is plausible, because photoexcitation of $NO_2^-\cdot H_2O\cdot Ar_3$ at 1200 cm^{-1} does induce a small branching into the three Ar atom loss channel, and thus, the $NO_2^-\cdot H_2O\cdot Ar$ fragment likely retains internal excitation on the order of the Ar binding energy, which is roughly 400 cm^{-1}. It is worth noting that such a convenient internal energy monitor is rare in cluster work.[41,42] Of course, we expect the internal energies of both isomers created as photofragments to be similar, since they are both governed by the evaporative ensemble ansatz.[43] The spectrum of the backside isomer (Figure 5b), on the other hand, is similar to that displayed by the backside $NO_2^-\cdot H_2O\cdot Ar$ isomer extracted from the source (Figure 3a, bands presented in blue). These seemingly disparate observations are seen to be internally consistent, however, when one considers the fact that the backside isomer does not exhibit the strong anharmonic coupling needed to yield significant oscillator strengths for the transitions with large changes in soft mode quanta, as is the case for the frontside complex.

Summarizing the results in the NO stretching region, we find the backside isomer to survive photoexcitation and remain intact in the fragment ions, which yields a novel and useful method for obtaining isomer-selective spectra. The frontside isomer also largely survives excitation through the NO stretching transition but yields new bands in the photoproduct that likely arise from internal excitation in the $NO_2^-\cdot H_2O\cdot Ar$ fragments. There is, in addition, a small feature in the fragment spectrum that occurs in the band location expected for the backside structure,

indicating that front-to-backside isomerization can be induced by excitation in the 1200 cm^{-1} range.

IIIC. Isomer Interconversion through the OH Stretching Modes. The absence of interconversion from back- to frontside isomers upon NO stretch excitation would seem to imply that the barrier for this process is >1200 cm^{-1}. However, on the basis of the calculations, we believe it to be more likely that the rate of Ar evaporation is faster than that for isomerization in this direction, which presents an intrinsic limitation to this method. It is also the case that the evidence for conversion from the front- to backside isomer rests on a rather weak band near 3000 cm^{-1}, and it would be useful to identify a regime where the isomerization reaction is both efficient and unambiguously established through the spectroscopic diagnostics. Since the relative rates should depend on the internal energy content, we extended the study to explore excitation through the higher-energy OH stretching modes. The nature of our approach dictates that we must also work with a larger number of attached Ar atoms in the $NO_2^-\cdot H_2O\cdot Ar_m$ parent ion, however, because we expect an average of five Ar atoms to be lost upon excitation of the cluster in the vicinity of the OH stretching transitions. We therefore focused this aspect of the study on the $NO_2^-\cdot H_2O\cdot Ar_6$ cluster because the dominant photofragment ion should retain a single Ar atom, which is required for spectroscopic interrogation of the product. Interestingly, there is a noticeable change in the relative contributions of the isomers to the NO stretching bands with increasing Ar solvation. Specifically, the 1230 cm^{-1} frontside transition, which is slightly larger than the backside 1203 cm^{-1} line in the spectrum of the $m = 1$ parent, is reduced by about a factor of 2 in the $m = 6$ spectrum. We have often encountered situations in which the isomer distribution is strongly dependent on the extent of Ar solvation[9,11,44] and have even used this to our advantage in several systems as a means with which to obtain isomer-selective spectra. For the present application, however, the diminishing population of the frontside isomer in the larger cluster is a disadvantage, and the situation is further complicated by significant broadening of its OH stretching pattern, which makes it difficult to exclusively excite this species. As a result, we were able to carry out an isomerization study only starting from the more abundant backside isomer.

In the case of OH stretching excitation, the higher power available for the pump laser led to a favorable situation in which we were able to interrogate its isomeric composition by probing the two nearby bands in the NO stretching region (i.e., the backside band at 1203 cm^{-1} and the frontside band at 1230 cm^{-1}). Figure 6 displays the low-energy spectrum of the $NO_2^-\cdot H_2O\cdot Ar$ fragment ion from the process,

$$NO_2^-\cdot H_2O\cdot Ar_6 + h\nu \rightarrow NO_2^-\cdot H_2O\cdot Ar + 5\ Ar \qquad (3)$$

with the pump laser tuned to excite the backside isomer at its strong 2975 cm^{-1} resonance corresponding to the fundamental of the ion-bound OH stretch [ν_{OH}^{IHB}(back) in Figure 3a]. The predissociation spectrum of the fragment ion does, indeed, display significant population in both isomers, with the higher energy band from the frontside isomer appearing with about one-third of the intensity as the band due to the backside species. With this observation, we have thus succeeded in driving the isomerization reaction in both directions.

The ability to drive isomerization in both directions is key to extracting the relative stability of the isomers as well as the magnitude of the barrier separating them, as discussed at length by Zwier and co-workers.[45−51] The observation of isomerization at 1200 cm^{-1} is consistent with our calculated barrier of ~1076 cm^{-1} from the reaction path displayed in Figure 4. Unfortunately, the large energy gap between the NO and OH stretching quanta allows for only a crude bracketing of the energetics, and the likely suppression of isomerization by Ar evaporation further complicates quantitative determination of these quantities. There is, on the other hand, an alternative available in the Ar-mediated scheme that can be used to establish the relative energies of the isomers, even when the isomerization rate is suppressed in one direction, as appears to be the case here. Specifically, the relative energetics are encoded in the number of Ar atoms evaporated when isomerization does or does not occur [$(m - n(\mathrm{I}))$ and $(m - n(\mathrm{II}))$ in eqs 1a and 1b, respectively], where the differences in Ar loss can be considered in the context of microcalorimetry.[52,53] Thus, the chemical energy from isomerization, ΔE (see Figure 1), should effectively add to the photon energy, $h\nu$, in determining the number of evaporation events, $n_{evap} \approx (\Delta E + h\nu)/\Delta H_{evap}$ (Ar). In the case of $NO_2^-\cdot H_2O\cdot Ar_6$, we note that, despite the observed ~30% conversion, the number of Ar atoms evaporated is as expected for the typical Ar binding energy of about 400 cm^{-1}. This observation indicates that the difference in energy between the two isomers is at most on the order of the argon binding energy and supports the interpretation that the failure to drive the back-to-frontside reaction at 1200 cm^{-1} excitation results from the kinetics rather than a large error in the calculated relative energies.

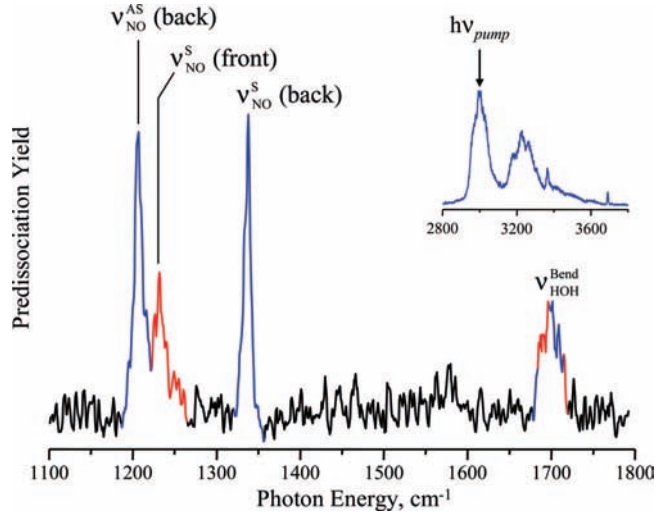

Figure 6. Argon predissociation spectrum of the $NO_2^-\cdot H_2O\cdot Ar$ photofragment produced by photoexcitation of $NO_2^-\cdot H_2O\cdot Ar_6$ (OH stretch spectrum shown in inset) with $h\nu_{pump}$ at 3000 cm^{-1}, which is the ion-bound OH stretch of the backside isomer. Approximately 30% conversion to the frontside isomer is evidenced by the presence of the NO_2^- asymmetric stretch at 1230 cm^{-1}, which is a characteristic feature of the frontside complex.

Our goal in the present study was to explore whether the relative rates of the intracluster processes described in eqs 1a and 1b allow an isomerization reaction to occur in a system that is unstable with respect to evaporation of a weakly bound solvent. The high efficiency of the isomerization reaction in the strongly bound $NO_2^-\cdot H_2O$ complex upon excitation at 3000 cm^{-1} establishes the viability of this approach. In fact, the detailed energetics of this system indicate that reaction can be observed even when the isomerization barrier is more than twice the Ar atom evaporation energy. This hierarchy of timescales is interesting because it enables a microscopic view of the exchange of energy between a reactive subsystem and surrounding solvent in a microcanonical regime. Moreover, this occurs in a sufficiently small system that the solvent bath states can be explicitly treated from a quantum perspective.

IV. Summary

We have introduced an Ar-cluster-mediated, pump−probe photoexcitation method involving three stages of mass selection to monitor isomerization reactions in size-selected cluster ions. This capability is demonstrated by carrying out vibrationally induced isomerization of a water molecule between two binding sites on the NO_2^- anion upon photoexcitation of the $NO_2^- \cdot H_2O$ complex within the Ar clusters $NO_2^- \cdot H_2O \cdot Ar_3$ and $NO_2^- \cdot H_2O \cdot Ar_6$. This is significant because it establishes that embedded systems can cross reaction barriers that are larger than the Ar binding energy. Specifically, photoexcitation in the NO stretch region near 1200 cm^{-1} gives a small amount of frontside-to-backside isomerization but no backside to frontside isomerization. The front-to-backside reaction can be driven, however, upon excitation in the OH stretch region near 3000 cm^{-1}. These observations are consistent with our calculations of the isomerization path, which place the barrier around 1100 cm^{-1}.

Acknowledgment. M.A.J. and K.D.J. thank the National Science Foundation for support of this work. In addition, M.A.J. acknowledges support from the Air Force Office of Scientific Research.

References and Notes

(1) Okumura, M.; Yeh, L. I.; Myers, J. D.; Lee, Y. T. *J. Chem. Phys.* **1986**, *85*, 2328.
(2) Ayotte, P.; Weddle, G. H.; Kim, J.; Johnson, M. A. *J. Am. Chem. Soc.* **1998**, *120*, 12361.
(3) Bailey, C. G.; Kim, J.; Dessent, C. E. H.; Johnson, M. A. *Chem. Phys. Lett.* **1997**, *269*, 122.
(4) Ayotte, P.; Bailey, C. G.; Weddle, G. H.; Johnson, M. A. *J. Phys. Chem. A* **1998**, *102*, 3067.
(5) Johnson, M. S.; Kuwata, K. T.; Wong, C.-K.; Okumura, M. *Chem. Phys. Lett.* **1996**, *260*, 551.
(6) Ayotte, P.; Kelley, J. A.; Nielsen, S. B.; Johnson, M. A. *Chem. Phys. Lett.* **2000**, *316*, 455.
(7) Diken, E. G.; Headrick, J. M.; Roscioli, J. R.; Bopp, J. C.; Johnson, M. A.; McCoy, A. B.; Huang, X.; Carter, S.; Bowman, J. M. *J. Phys. Chem. A* **2005**, *109*, 571.
(8) Robertson, W. H.; Price, E. A.; Weber, J. M.; Shin, J.-W.; Weddle, G. H.; Johnson, M. A. *J. Phys. Chem. A* **2003**, *107*, 6527.
(9) Myshakin, E. M.; Jordan, K. D.; Robertson, W. H.; Weddle, G. H.; Johnson, M. A. *J. Chem. Phys.* **2003**, *118*, 4945.
(10) Kolaski, M.; Lee, H. M.; Choi, Y. C.; Kim, K. S.; Tarakeshwar, P.; Miller, D. J.; Lisy, J. M. *J. Chem. Phys.* **2007**, 126.
(11) Roscioli, J. R.; Hammer, N. I.; Johnson, M. A.; Diri, K.; Jordan, K. D. *J. Chem. Phys.* **2008**, *128*, 104314.
(12) Elliott, B. M.; Relph, R. A.; Roscioli, J. R.; Bopp, J. C.; Gardenier, G. H.; Guasco, T. L.; Johnson, M. A. *J. Chem. Phys.* **2008**, in press.
(13) Ensminger, F. A.; Plassard, J.; Zwier, T. S.; Hardinger, S. *J. Chem. Phys.* **1993**, *99*, 8341.
(14) Becke, A. D. *J. Chem. Phys.* **1993**, *98*, 5648.
(15) Lee, C.; Yang, W.; Parr, R. G. *Phys. Rev. B* **1988**, *37*, 785.
(16) Stephens, P. J.; Devlin, F. J.; Chabalowski, C. F.; Frisch, M. J. *J. Phys. Chem.* **1994**, *98*, 11623.
(17) Becke, A. D. *Phys. Rev. A* **1988**, *38*, 3098.
(18) Kendall, R. A.; Dunning, T. H., Jr.; Harrison, R. J. *J. Chem. Phys.* **1992**, *96*, 6796.
(19) Woon, D. E.; Dunning, T. H., Jr. *J. Chem. Phys.* **1993**, *98*, 1358.
(20) Johnson, M. A. Stanford University, 1983.
(21) Smith, J. M.; Zhang, X.; Knee, J. L. *J. Chem. Phys.* **1993**, *99*, 2550.
(22) Paik, D. H.; Lee, I.-R.; Yang, D.-S.; Baskin, J. S.; Zewail, A. H. *Science* **2004**, *306*, 672.
(23) Johnson, M. A.; Lineberger, W. C. Pulsed Methods for Cluster Ion Spectroscopy. In *Techniques for the Study of Ion−Molecule Reactions*; Farrar, J. M., Saunders, W. H., Jr., Eds.; Wiley: New York, 1988; Vol. XX; p 591.
(24) Robertson, W. H.; Kelley, J. A.; Johnson, M. A. *Rev. Sci. Instrum.* **2000**, *71*, 4431.
(25) Stearns, J. A.; Das, A.; Zwier, T. S. *Phys. Chem. Chem. Phys.* **2004**, *6*, 2605.
(26) Gerhards, M.; Unterberg, C.; Gerlach, A. *Phys. Chem. Chem. Phys.* **2002**, *4*, 5563.
(27) Myshakin, E. M.; Sibert, E. L., III; Johnson, M. A.; Jordan, K. D. *J. Chem. Phys.* **2003**, *119*, 10138.
(28) Head-Gordon, M.; Pople, J. A.; Frisch, M. J. *Chem. Phys. Lett.* **1988**, *153*, 503.
(29) Peng, C.; Schlegel, H. B. *Isr. J. Chem.* **1993**, *33*, 449.
(30) Forney, D.; Thompson, W. E.; Jacox, M. E. *J. Chem. Phys.* **1993**, *99*, 7393.
(31) Cizek, J. *Adv. Chem. Phys.* **1969**, *14*, 35.
(32) Purvis, G. D.; Bartlett, R. J. *J. Chem. Phys.* **1982**, *76*, 1910.
(33) Scuseria, G. E.; Janssen, C. L.; Schaefer, H. F. *J. Chem. Phys.* **1988**, *89*, 7382.
(34) Scuseria, G. E.; Schaefer, H. F., III *J. Chem. Phys.* **1989**, *90*, 3700.
(35) Pople, J. A.; Head-Gordon, M.; Raghavachari, K. *J. Chem. Phys.* **1987**, *87*, 5968.
(36) Hirao, K. *Chem. Phys. Lett.* **1993**, *201*, 59.
(37) Frisch, M. J.; Trucks, G. W.; Schlegel, H. B.; Scuseria, G. E.; Robb, M. A.; Cheeseman, J. R.; Montgomery, J. A., Jr.; Vreven, T.; Kudin, K. N.; Burant, J. C.; Millam, J. M.; Iyengar, S. S.; Tomasi, J.; Barone, V.; Mennucci, B.; Cossi, M.; Scalmani, G.; Rega, N.; Petersson, G. A.; Nakatsuji, H.; Hada, M.; Ehara, M.; Toyota, K.; Fukuda, R.; Hasegawa, J.; Ishida, M.; Nakajima, T.; Honda, Y.; Kitao, O.; Nakai, H.; Klene, M.; Li, X.; Knox, J. E.; Hratchian, H. P.; Cross, J. B.; Adamo, C.; Jaramillo, J.; Gomperts, R.; Stratmann, R. E.; Yazyev, O.; Austin, A. J.; Cammi, R.; Pomelli, C.; Ochterski, J. W.; Ayala, P. Y.; Morokuma, K.; Voth, G. A.; Salvador, P.; Dannenberg, J. J.; Zakrzewski, V. G.; Dapprich, S.; Daniels, A. D.; Strain, M. C.; Farkas, O.; Malick, D. K.; Rabuck, A. D.; Raghavachari, K.; Foresman, J. B.; Ortiz, J. V.; Cui, Q.; Baboul, A. G.; Clifford, S.; Cioslowski, J.; Stefanov, B. B.; Liu, G.; Liashenko, A.; Piskorz, P.; Komaromi, I.; Martin, R. L.; Fox, D. J.; Keith, T.; Al-Laham, M. A.; Peng, C. Y.; Nanayakkara, A.; Challacombe, M.; Gill, P. M. W.; Johnson, B.; Chen, W.; Wong, M. W.; Gonzalez, C.; Pople, J. A. *Gaussian 03*, revision C.02; Gaussian, Inc.: Wallingford, CT, 2003.
(38) Werner, H.-J.; Knowles, P. J.; Lindh, R.; Manby, F. R.; Schütz, M.; Celani, P.; Korona, T.; Mitrushenkov, A.; Rauhut, G.; Adler, T. B.; Amos, R. D.; Bernhardsson, A.; Berning, A.; Cooper, D. L.; Deegan, M. J. O.; Dobbyn, A. J.; Eckert, F.; Goll, E.; Hampel, C.; Hetzer, G.; Hrenar, T.; Knizia, G.; Köppl, C.; Liu, Y.; Lloyd, A. W.; Mata, R. A.; May, A. J.; McNicholas, S. J.; Meyer, W.; Mura, M. E.; Nicklass, A.; Palmieri, P.; Pflüger, K.; Pitzer, R.; Reiher, M.; Schumann, U.; Stoll, H.; Stone, A. J.; Tarroni, R.; Thorsteinsson, T.; Wang, M.; Wolf, A. *MOLPRO, version 2006.1, a package of ab initio programs;* http://www.molpro.net.
(39) Campagnola, P. J.; Posey, L. A.; Johnson, M. A. *J. Chem. Phys.* **1991**, *95*, 7998.
(40) McCunn, L. R.; Headrick, J.; Johnson, M. A. *Phys. Chem. Chem. Phys.* **2008**, *10*, 3118.
(41) Han, C.-C.; Johnson, M. A. *Chem. Phys. Lett.* **1992**, *189*, 460.
(42) Li, R.; Hanold, K. A.; Garner, M. C.; Luong, A. K.; Continetti, R. E. *Faraday Discuss.* **1997**, *108*, 115.
(43) Klots, C. E. *J. Chem. Phys.* **1985**, *83*, 5854.
(44) Hammer, N. I.; Roscioli, J. R.; Johnson, M. A. *J. Phys. Chem. A* **2005**, *109*, 7896.
(45) Dian, B. C.; Clarkson, J. R.; Zwier, T. S. *Science* **2004**, *303*, 1169.
(46) Clarkson, J. R.; Baquero, E.; Shubert, V. A.; Myshakin, E. M.; Jordan, K. D.; Zwier, T. S. *Science* **2005**, *307*, 1443.
(47) Selby, T. M.; Clarkson, J. R.; Mitchell, D.; Fitzpatrick, J. A. J.; Lee, H. D.; Pratt, D. W.; Zwier, T. S. *J. Phys. Chem. A* **2005**, *109*, 4484.
(48) Clarkson, J. R.; Dian, B. C.; Moriggi, L.; DeFusco, A.; McCarthy, V.; Jordan, K. D.; Zwier, T. S. *J. Chem. Phys.* **2005**, 122.
(49) Clarkson, J. R.; Baquero, E.; Zwier, T. S. *J. Chem. Phys.* **2005**, 122.
(50) Zwier, T. S. *J. Phys. Chem. A* **2006**, *110*, 4133.
(51) LeGreve, T. A.; Clarkson, J. R.; Zwier, T. S. *J. Phys. Chem. A* **2008**, *112*, 3911.
(52) Posey, L. A.; DeLuca, M. J.; Campagnola, P. J.; Johnson, M. A. *J. Phys. Chem.* **1989**, *93*, 1178.
(53) Arnold, S. T.; Morris, R. A.; Viggiano, A. A.; Johnson, M. A. *J. Phys. Chem.* **1996**, *100*, 2900.

JP808283R